PASJ: Publ. Astron. Soc. Japan **53**, –15 (2002)

Nonlinear Stochastic Biasing of Peaks and Halos: Scale-Dependence, Time-Evolution, and Redshift-Space Distortion from Cosmological N-body Simulations

Atsushi TARUYA[1], Hiromitsu MAGIRA[1], Y.P. JING[2,3,4,5], and Yasushi SUTO,[1,2]

[1] *Department of Physics, School of Science, University of Tokyo, Tokyo 113-0033*
E-mail(AT): ataruya@utap.phys.s.u-tokyo.ac.jp
[2] *Research Center for the Early Universe, School of Science, University of Tokyo, Tokyo 113-0033*
[3] *Theory Division, National Astronomical Observatory, Mitaka 181-8588*
[4] *Shanghai Astronomical Observatory, the Partner Group of MPI für Astrophysik, Nandan Road 80, Shanghai 20030, China*
[5] *National Astronomical Observatories, Chinese Academy of Sciences, Beijing 100012,China*

(Received 2000 April 11; accepted 2000 December 26)

Abstract

We quantify the degree of nonlinearity and stochasticity of the clustering of biased objects, using cosmological N-body simulations. Adopting the peaks and the halos as representative biasing models, we focus on the two-point correlation of the biased objects, dark matter and their cross-correlation. Especially, we take account of the effect of redshift-space distortion and attempt to clarify the scale-dependence and the time-dependence by analyzing the biasing factor and the cross-correlation factor. On small scales, stochasticity and nonlinearity become appreciable and strongly object-dependent, especially in redshift space due to the pair-wise velocity dispersion of the biased objects. Nevertheless, an approximation of deterministic linear biasing $\delta_{\rm obj} \simeq b_{\rm obj}\delta_{\rm mass}$ works reasonably well even in the quasi-linear regime $r \gtrsim 10h^{-1}$ Mpc, and linear redshift-space distortion explains the clustering amplitudes in redshift space in this regime.

Key words: Cosmology: dark matter - Galaxies:clustering - halos - Large-scale structure of universe - Theory

1. Introduction

Luminous objects, such as galaxies and quasars, are not direct tracers of the mass in the universe. In fact, the difference of the spatial distribution between luminous objects and dark matter, or the *bias*, has been indicated from a variety of observations. In order to confront theoretical model predictions for the *mass* distribution against observational data, one needs a relation of density fields of mass and luminous objects. Consider the density contrasts of visible objects and mass, $\delta_{\rm obj}(\mathbf{x}, z|R)$ and $\delta_{\rm mass}(\mathbf{x}, z|R)$, at a position $\mathbf{x}$ and a redshift z smoothed over a scale R. In general, the former should depend on various other auxiliary variables $\vec{\mathcal{A}}$ defined at different locations $\mathbf{x}'$ and redshifts z' smoothed over different scales R' in addition to the mass density contrast at the same position, $\delta_{\rm mass}(\mathbf{x}, z|R)$. While this relation can be schematically expressed as

$$\delta_{\rm obj}(\mathbf{x}, z|R) = \mathcal{F}[\mathbf{x}, z, R, \delta_{\rm mass}(\mathbf{x}, z|R), \vec{\mathcal{A}}(\mathbf{x}', z'|R'), \ldots], \tag{1}$$

it is impossible even to specify the list of the astrophysical variables $\vec{\mathcal{A}}$, and thus hopeless to predict the functional form in a rigorous manner. Therefore if one simply focuses on the relation between $\delta_{\rm obj}(\mathbf{x}, z|R)$ and $\delta_{\rm mass}(\mathbf{x}, z|R)$, the relation becomes inevitably *stochastic* and *nonlinear* due to the dependence on unspecified auxiliary variables $\vec{\mathcal{A}}$.

For illustrative purposes, define the *biasing* factor as the ratio of the density contrasts of luminous objects and mass:

$$B_{\rm obj}(\mathbf{x}, z|R) \equiv \frac{\delta_{\rm obj}(\mathbf{x}, z|R)}{\delta_{\rm mass}(\mathbf{x}, z|R)} = \frac{\mathcal{F}[\mathbf{x}, z, R, \delta_{\rm mass}(\mathbf{x}, z|R), \vec{\mathcal{A}}(\mathbf{x}', z'|R'), \ldots]}{\delta_{\rm mass}(\mathbf{x}, z|R)}. \tag{2}$$

Only in very idealized situations, the above *nonlocal stochastic nonlinear* factor in terms of $\delta_{\rm mass}$ may be approximated by

1. a *local stochastic nonlinear* bias:

$$B_{\rm obj}(\mathbf{x}, z|R) = b^{\rm (sn)}_{\rm obj}[\mathbf{x}, z, R, \delta_{\rm mass}(\mathbf{x}, z|R), \vec{\mathcal{A}}(\mathbf{x}, z|R), \ldots], \tag{3}$$

2. a *local deterministic nonlinear* bias:

$$B_{\rm obj}(\mathbf{x}, z|R) = b^{\rm (dn)}_{\rm obj}[z, R, \delta_{\rm mass}(\mathbf{x}, z|R)], \tag{4}$$

and

3. a *local deterministic linear* bias:

$$B_{\rm obj}(\mathbf{x}, z|R) = b_{\rm obj}(z, R) \tag{5}$$

From the above point of view, the local deterministic linear bias is obviously unrealistic, but is still a widely used conventional model for biasing. In fact, the time- and scale-dependence of the linear bias factor $b_{\rm obj}(z, R)$ was neglected in many previous studies of biased galaxy formation until very recently. Currently, however, various models beyond the deterministic linear biasing have been seriously considered with particular emphasis on the nonlinear and stochastic aspects of the biasing (Pen 1998; Tegmark, Peebles 1998; Dekel, Lahav 1999; Taruya, Koyama, Soda 1999; Tegmark, Bromley 1999; Blanton et al. 1999; Somerville et al. 1999; Blanton et al. 2000; Taruya 2000; Taruya, Suto 2000; Yoshikawa et al. 2000).

In the present paper, we examine two fairly simplified but well-defined popular models for biasing, i.e., peaks and halos, paying particular attention to their stochastic and nonlinear nature on the basis of cosmological N-body simulations. Especially we take account of the redshift-space distortion effect on biasing which has not been studied in previous work. Our main purpose is to find the validity and limitation of the local deterministic linear approximation $\delta_{\rm obj} = b_{\rm obj}\delta_{\rm mass}$ for the general stochastic and nonlinear biasing. By analyzing the two-point statistics of the biased objects and the mass distribution, we quantitatively measure the stochasticity and nonlinearity and investigate the scale-dependence and the time-evolution of clustering amplitude both in real and redshift spaces.

The nonlinear stochastic biasing for two-point statistics is not a simple theoretical issue, but important in the proper comparison with observation. Although the biasing properties for one-point statistics have been extensively discussed in literature using numerical simulations and/or analytic models, a similar investigation of biasing in two-point statistics has not yet performed. This is because nonlinear stochastic biasing was originally formulated using the one-point statistics. In this paper, we quantify the biasing features of clustering in terms of the two-point correlation function. In particular, we focus on the biasing factor $b_{\rm obj}$ and the cross correlation coefficient $r_{\rm obj}$ defined by equations.(7) and (8). Those quantities are related and compared to the biasing parameters defined in terms of the one-point statistics.

The paper is organized as follows. In section 2, we briefly describe the simulated catalogues and evaluate the two-point correlation functions for the peaks and dark halos. We then examine the scale-dependence and the time-evolution of biasing measured from those statistics in section 3. In particular we pay attention to the difference of the biasing properties of peaks and halos. The results are compared with simple theoretical models and predictions from linear theory of redshift-space distortion. In addition, we calculate the variances of peaks, halos and dark matter particles taking into account the point process. Section 4 is devoted to the conclusions and discussion.

2. Peak and halo catalogues from cosmological N-body simulations

2.1. Simulations

In this paper, we use a series of cosmological N-body simulations in cold dark matter (CDM) cosmogonies (Jing, Suto 1998), whose parameters are listed in Table 1. All the models employ $N = 256^3$ dark matter particles in the periodic comoving cube of the boxsize $L_{\rm box} = 300h^{-1}$Mpc, and are evolved on the basis of the Particle-Particle – Particle-Mesh ($\rm P^3M$) method. The initial conditions of the particle distribution match the CDM transfer function of Bardeen et al. (1986) characterized by the shape parameter, Γ. The RMS mass fluctuation amplitude at $8h^{-1}$Mpc, σ_8, is normalized according to the cluster abundance (Kitayama, Suto 1997). We analyze three realizations for each cosmological model at $z = 0$ and $z = 2.2$, and one realization for LCDM model at $z = 0.6$, 1.0, and $z = 3.4$ to examine the time evolution.

As specific models of biasing, we consider two popular cases; primordial density peaks and dark matter halos. The density peaks are selected according to the algorithm of Mo, Jing & White (1997). The initial density field

is smoothed with a Gaussian window. The filtering radius of $R_{\rm f} = 0.54\,h^{-1}\,$Mpc is adopted for the smoothing so that the typical size of the peaks becomes relevant for galactic-sized objects (Bardeen et al. 1986). Given a density field and a threshold peak height, this algorithm predicts the number of the peaks that each simulation dark matter particle will carry. The number of peaks per dark matter particle in our simulations is always less than 1. So we have picked up the peaks by randomly selecting simulation particles with the selection probability set equal to its number of the peaks for each particle. This way guarantees that a correct total number of peaks is reproduced for the Gaussian random field. Those peak particles subsequently move according to the gravitational field, and thus their total number is conserved. We choose $\nu_{\rm th} = 1.0$, 2.0, and 3.0 as the threshold of the peak height ν (Table 2). As for the dark matter halos, these are identified using the standard friend-of-friend algorithm with a linking length of 0.2 in units of the mean particle separation. We select halos of mass larger than the threshold $M_{\rm th} = 2.0 \times 10^{12}$, 5.0×10^{12} and $1.0 \times 10^{13}\,h^{-1}\,M_\odot$ (Table 3). The halos having the dark matter particle $N_{\rm mass} < 10$ have been excluded.

Figure 1 depicts the distribution of dark matter particles (*upper-panel*), peaks (*middle-panel*) and halos (*lower-panel*) in LCDM model at $z = 0$ and $z = 2.2$ within a circular slice (*comoving* radius of $150h^{-1}$Mpc and thickness of $15h^{-1}$Mpc). We locate a fiducial observer in the center of the circle. Then the *comoving* position vector $\mathbf{r}$ for a particle with a *comoving* peculiar velocity $\mathbf{v}$ at a redshift z is observed at the position s in redshift space:

$$\mathbf{s} = \mathbf{r} + \frac{1}{H(z)}\,\frac{\mathbf{r}\cdot\mathbf{v}}{|\mathbf{r}|}\,\frac{\mathbf{r}}{|\mathbf{r}|}, \tag{6}$$

where $H(z)$ is the Hubble parameter at z. The right panels in Figure 1 plot the observed distribution in redshift space, where the redshift-space distortion is quite visible; the coherent velocity field enhances the structure perpendicular to the line-of-sight of the observer (*squashing*) while the virialized clump becomes elongated along the line-of-sight (*finger-of-God*). Although the distribution of peaks in Figure 1a and 1b seems rather different, this is simply due to the strong concentration along the filamentary regions in Figure 1a, and the total number of peaks is the same. Figure 1 qualitatively illustrates that the redshift-space distortion is sensitively dependent on the objects, and this is what we will attempt to quantify statistically in the rest of paper.

2.2. Two-point statistics

We use the two-point correlation functions to quantify stochasticity and nonlinearity in biasing of peaks and halos, and explore the signature of the redshift-space distortion. Since we are interested in the relation of the biased objects and the dark matter, we introduce three correlation functions; the auto-correlation functions of dark matter and the objects, $\xi_{\rm mm}$ and $\xi_{\rm oo}$, and their cross-correlation function $\xi_{\rm om}$. In the present case, the subscript o refers to either h (halos) or ν (peaks). We also use the superscripts R and S to distinguish quantities defined in real and redshift spaces, respectively. We estimate those correlation functions using the standard pair-count method. The correlation function $\xi^{(S)}$ is evaluated under the distant-observer approximation.

Those correlation functions are plotted in Figures 2 and 3 for peaks and halos, respectively. Their qualitative behavior in redshift space is already well-known and easy to understand (e.g, Kaiser 1987; Hamilton 1998). The correlation functions of biased objects generally are larger than those of mass amplitudes. In nonlinear regimes ($\xi > 1$) the finger-of-god effect suppresses the amplitude of $\xi^{(\rm S)}$ relative to $\xi^{(\rm R)}$, while $\xi^{(\rm S)}$ is larger than $\xi^{(\rm R)}$ in linear regimes ($\xi < 1$) due to the coherent velocity field. In the next section, we present more quantitative analysis in terms of the stochastic nonlinear biasing scheme and compare with the existing theoretical predictions valid in linear regimes.

3. Scale-dependence and time-evolution of biasing parameters

In order to quantify the behavior of biasing, we introduce the biasing factor and the cross-correlation factor:

$$b_{\rm obj}(r,z) \equiv \sqrt{\frac{\xi_{\rm oo}}{\xi_{\rm mm}}}, \tag{7}$$

$$r_{\rm obj}(r,z) \equiv \frac{\xi_{\rm mo}}{\sqrt{\xi_{\rm oo}\xi_{\rm mm}}}, \tag{8}$$

following their counterparts defined in terms of the one-point statistics (e.g., Pen 1998; Tegmark, Peebles 1998; Dekel, Lahav 1999; Taruya, Koyama, Soda 1999; Taruya 2000). In equations (7) and (8), $b_{\rm obj}$ measures the relative strength

of the clustering of objects and $r_{\rm obj}$ characterizes the degree of nonlinearity and stochasticity of the underlying biasing mechanism (Dekel, Lahav 1999). The deterministic linear bias $\delta_{\rm obj} = b_{\rm obj}\delta_{\rm mass}$, for instance, implies that $r_{\rm obj} = 1$.

Since the two-point correlation functions are not positive definite, however, the physical interpretations of the above definitions are somewhat ambiguous in that case. We will discuss this point in detail in Sec.3.4 where we relate them to those defined by the one-point statistics, i.e, $b^{(1)}_{\rm obj}$ and $r^{(1)}_{\rm obj}$. In any case, this does not happen in our analysis below on scales of cosmological interest, and we adopt the above "conventional" definitions. In what follows, we focus on the scale-dependence, time-evolution of the above parameters, as well as on their behavior in redshift space. Before presenting the simulation results, we briefly summarize the existing theoretical models. They turn out to be useful in comparing and understanding our results despite that they are valid mainly in linear regimes.

3.1. Theoretical models for biasing

3.1.1. Peak model

Density peaks are the first physical model of cosmological biasing proposed by Kaiser (1984), and then extensively studied by Bardeen et al. (1986). According to the latter, we consider the density peaks in the *primordial* random Gaussian field smoothed with a Gaussian window function. Then the height of each peak is defined as the ratio of the density contrast at the position smoothed with $R_{\rm f}$ and its RMS value, $\nu = \delta/\sigma_0$. Although δ and σ_0 in this context should refer to the values at some initial epoch, we take another (but equivalent) view that their values are linearly extrapolated to the present time. To be more specific, σ_0 is computed by setting $l = 0$ in the following general expression for the l-th order moment:

$$\sigma_l^2(R_{\rm f}) \equiv \int \frac{d^3k}{(2\pi)^3}\, k^{2l}\, P(k; z=0)\, \exp\left(-k^2 R_{\rm f}^2\right), \tag{9}$$

where $P(k; z=0)$ is the linearly extrapolated power spectrum.

Bardeen et al. (1986) showed that the number density of peaks, $n_{\rm peak}$, is given by

$$n_{\rm peak}(\nu) = \frac{1}{(2\pi)^2 R_*^3} e^{-\nu^2/2} G(\gamma, \gamma\nu), \tag{10}$$

where

$$R_* = \sqrt{3}\frac{\sigma_1(R_{\rm f})}{\sigma_2(R_{\rm f})}, \tag{11}$$

$$\gamma = \frac{\sigma_1^2(R_{\rm f})}{\sigma_0(R_{\rm f})\sigma_2(R_{\rm f})}, \tag{12}$$

$$G(\gamma, y) = \int_0^\infty dx\, F(x)\, \frac{\exp[-(x-y)^2/2(1-\gamma^2)]}{[2\pi(1-\gamma^2)]^{1/2}}, \tag{13}$$

$$F(x) = \frac{x^3 - 3x}{2}\left\{ {\rm erf}\left[\sqrt{\frac{5}{2}}\, x\right] + {\rm erf}\left[\sqrt{\frac{5}{2}}\,\frac{x}{2}\right]\right\} + \sqrt{\frac{2}{5\pi}}\left[\left(\frac{31}{4}x^2 + \frac{8}{5}\right) e^{-5x^2/8} + \left(\frac{x^2}{2} - \frac{8}{5}\right) e^{-5x^2/2}\right]. \tag{14}$$

Mo, Jing & White (1997) derived a formula which relates the number density fluctuations of peaks to the mass density fluctuations $\delta_{\rm mass}$ at z. Denoting $D(z)$ as the linear growth factor normalized to unity at $z = 0$, the extrapolated amplitude of mass fluctuations at the present time is $\delta_{\rm mass}/D(z)$. Then, the fluctuation $\delta_{\rm peak}$ with $\nu \gg \delta_{\rm mass}/[D(z)\sigma_0]$ is given by

$$\delta_{\rm peak}(\nu, z) = (1+\delta_{\rm mass})\frac{n_{\rm peak}(\nu)|_{\nu\to\nu-\delta_{\rm mass}/[D(z)\sigma_0]}}{n_{\rm peak}(\nu)} - 1 \simeq \left\{1 - \frac{1}{D(z)\sigma_0}\frac{d}{d\nu}\log\left[n_{\rm peak}(\nu)\right]\right\}\delta_{\rm mass}, \tag{15}$$

in the limit of linear theory. Thus the peak model reduces to the scale-independent deterministic linear biasing:

$$b_{\rm peak}(\nu, z) \equiv \frac{\delta_{\rm peak}}{\delta_{\rm mass}} = 1 + \frac{1}{D(z)}\,\frac{\nu^2 + g_1}{\sigma_0(R_{\rm f})\nu}, \tag{16}$$

$$g_1 \equiv -\frac{\gamma\nu}{G(\gamma,\gamma\nu)}\,\frac{\partial G(\gamma, y)}{\partial y}\bigg|_{y=\gamma\nu}. \tag{17}$$

Since our simulation data are for peaks with the peak height above ν, we use the following effective biasing factor in the comparison below:

$$b_{\rm peak,eff}(>\nu,z) = \frac{\displaystyle\int_\nu^\infty b_{\rm peak}(\nu',z)n_{\rm peak}(\nu')d\nu'}{\displaystyle\int_\nu^\infty n_{\rm peak}(\nu')d\nu'}. \tag{18}$$

3.1.2. Halo biasing (Merging model)

Another popular model of cosmological biasing is that one dark matter halo accommodate a single luminous object. This is established as a fairly realistic model for clusters of galaxies (e.g, Kitayama, Suto 1996), and may provide a reasonable approximation even for bright galaxies (Somerville et al. 2000). The number density of halos with mass M at z is well approximated by the Press–Schechter mass function (Press, Schechter 1974):

$$n_{\rm halo}(M,z)dM = \frac{1}{\sqrt{2\pi}}\frac{\bar\rho}{M}\frac{\delta_c}{\Delta^3(M,z)}\exp\left[-\frac{\delta_c^2}{\Delta^2(M,z)}\right]\left|\frac{d\Delta^2(M,z)}{dM}\right|dM, \tag{19}$$

$$\Delta^2(M,z) = D^2(z)\int\frac{d^3k}{(2\pi)^3}P(k;z=0)\,\frac{9}{(kR_{\rm TH})^6}\left[\sin(kR_{\rm TH})-kR_{\rm TH}\cos(kR_{\rm TH})\right]^2, \tag{20}$$

where $\bar\rho$ is the mean mass density, δ_c is the critical density threshold of the spherical collapse, and the spherical top-hat radius $R_{\rm TH}$ is $(3M/4\pi\bar\rho)^{1/3}$.

An analytic model for dark halo biasing is constructed in a similar way as the peak model (Mo, White 1996; Mo et al. 1997), yielding

$$\delta_{\rm halo}(M,z) = (1+\delta_{\rm mass})\frac{n_{\rm halo}(M,z)|_{\delta_c\to\delta_c-\delta_{\rm mass}}}{n_{\rm halo}(M,z)} - 1 \simeq \left\{1-\frac{d}{d\delta_c}\log\left[n_{\rm halo}(M,z)\right]\right\}\delta_{\rm mass}. \tag{21}$$

Again in the above limit of linear regime, the halo biasing becomes linear, deterministic and scale-independent. In what follows, we adopt the fitting formula of Jing (1998) for $b_{\rm halo}(M,z)$ which incorporates a correction factor for low mass halos:

$$b_{\rm halo}(M,z) = \left(\frac{0.5}{\nu_{\rm h}^4}+1\right)^{(0.06-0.02n_{\rm eff})}\left(1+\frac{\nu_{\rm h}^2-1}{\delta_c}\right), \tag{22}$$

$$\nu_{\rm h} = \frac{\delta_c}{\Delta(M,z)}, \tag{23}$$

$$n_{\rm eff} = \left.\frac{d\ln P(k)}{d\ln k}\right|_{k=2\pi/R}, \tag{24}$$

and introduce the effective halo biasing factor to compare with the simulation results:

$$b_{\rm halo,eff}(>M,z) = \frac{\displaystyle\int_M^\infty b_{\rm halo}(M',z)\,n_{\rm halo}(M',z)dM'}{\displaystyle\int_M^\infty n_{\rm halo}(M',z)dM'}. \tag{25}$$

3.1.3. Time-evolution of biasing parameters in a number-conserving model

As noted above, both peak and halo models result in linear, deterministic and scale-independent biasing on large scales. In this limit, time-evolution of the biasing parameters can be generally computed using the continuity equation if the number of objects is constant (number conserving model). This is indeed the case for the peak model, while not for the halo model.

The explicit expression for the time-dependent biasing factor is obtained first by Fry (1996) in a context of the deterministic biasing model. This is later extended to the stochastic biasing case in the linear regime by Tegmark & Peebles (1998), and then in the weakly nonlinear regime by Taruya, Koyama & Soda (1999) and Taruya (2000).

We use the expression of Tegmark & Peebles (1998) in considering the evolution of peak bias, which relates ($b_{\rm obj}$, $r_{\rm obj}$) at a given redshift z_1 to those at an earlier epoch, $z_2 (> z_1)$:

$$b_{\rm obj}(z_1) = \frac{\sqrt{D^2(z_2,z_1) - 2D(z_2)b_{\rm obj}(z_2)r_{\rm obj}(z_2)D(z_2,z_1) + D^2(z_2)b_{\rm obj}(z_2)^2}}{D(z_1)}, \tag{26}$$

$$r_{\rm obj}(z_1) = \frac{D(z_2)b_{\rm obj}(z_2)r_{\rm obj}(z_2) - D(z_2,z_1)}{D(z_1)b_{\rm obj}(z_1)}, \tag{27}$$

where we define

$$D(z_2,z_1) \equiv D(z_2) - D(z_1). \tag{28}$$

We note that in the case of a deterministic linear bias, $r_{\rm obj}$ becomes unity and the above expression reduces to

$$b_{\rm obj}(z_1) = 1 + \frac{D(z_2)}{D(z_1)}\left[b_{\rm obj}(z_2) - 1\right], \tag{29}$$

which is identical to the behavior of $b_{\rm peak}$ (eq.[16]) in a linear regime.

3.2. Scale-dependence

With the above theoretical predictions as a reference, let us examine the scale-dependence of the biasing parameters. Figures 4 and 5 display the results for peak and halo models, respectively. Apart from the object-dependent amplitude of the parameters, the general trend is quite similar; on large scales, $r_{\rm obj}^{(R)}$ is close to unity and the deterministic linear bias is a reasonable approximation in this linear regime. In fact, both $b_{\rm peak}^{(R)}$ and $b_{\rm halo}^{(R)}$ approach the predictions (18) and (25), respectively, as the separation r increases. On smaller scales, the biasing becomes nonlinear and stochastic (i.e., $r_{\rm obj}^{(R)} < 1$) and the clustering amplitude relative to mass becomes generally stronger ($b_{\rm obj}^{(R)}$ increases). Although $b_{\rm halo}^{(R)}$ levels off and then *decreases* below a few Mpc, this should be mainly ascribed to the exclusion effect due to the finite halo size (Mo, Jing, White 1997).

Turn next to the redshift-space distortion effect on the scale-dependence. On large scales, the simulation results are understood fairly reasonably with a straightforward extension of a linear distortion model (Kaiser 1987) to the stochastic biasing model, which is described in Appendix; we obtain $b_{\rm obj}^{(S)} \lesssim b_{\rm obj}^{(R)}$ and $r_{\rm obj}^{(S)} \simeq r_{\rm obj}^{(R)}$. On small scales, however, the degree of the redshift-space distortion depends sensitively on the nature of biased objects. Note that the redshift-space distortion even leads to $r_{\rm halo}^{(S)} \gtrsim 1$, but this is simply due to the improper definition on small scales (see discussion in Section 3.4). We also find that while $b_{\rm peak}^{(S)}$ is significantly suppressed with respect to $b_{\rm peak}^{(R)}$, the amplitude of $b_{\rm halo}^{(S)}$ is comparable to that of $b_{\rm halo}^{(R)}$. For the latter aspect, this implies that the pair-wise velocity dispersion, $\langle v_{12,{\rm obj}}^2 \rangle$, on small scales is dependent on objects, and that $\langle v_{12,{\rm halo}}^2 \rangle \lesssim \langle v_{12,{\rm mass}}^2 \rangle \lesssim \langle v_{12,{\rm peak}}^2 \rangle$. We directly compute the velocity dispersion and indeed confirm that the above relation holds in our simulation catalogues of peaks and halos.

3.3. Time evolution

Now we examine the time evolution of the biasing parameters. For this purpose, we consider the LCDM model and plot the biasing parameters as a function of the redshift in Figure 6. In order to probe the linear, quasi-nonlinear and nonlinear scales of the gravitational clustering, we select three separation lengths; $r = 1$, 5 and $23\,h^{-1}$Mpc for peaks, and $r = 7$, 13 and $23\,h^{-1}$Mpc for halos. Again the qualitative behavior is quite similar in the peak and halo models regardless of the scale. Toward lower redshifts, $r_{\rm obj}$ increases and approaches unity while $b_{\rm obj}$ decreases. We plot the number-conserving model predictions (Tegmark, Peebles 1998) in Figure 6a using the values of simulations at $z_2 = 3.4$ for $b_{\rm peak}(z_2)$ and $r_{\rm peak}(z_2)$ in equations (26) and (27). It turns out that the time evolution of biasing in peak model is well described by the number-conserving model even on fairly nonlinear scales.

Figure 6b plots the results in halo model. Since our halo catalogues are selected by the mass, the number density of the selected halos changes with redshift according to the Press-Schechter mass function. Therefore the number-conserving model predictions do not match the results. Rather we plot the bias formula by Jing (1998) which seem to be in reasonable agreement with the evolution in simulations. Incidentally we create a different halo catalogue which conserves the number density by appropriately changing the selection mass threshold with z, and make sure that the evolution in such halo catalogues agrees well with the number-conserving model prediction.

3.4. Comparison with biasing parameters in terms of the one-point statistics

As noted earlier, the biasing parameters defined in equations (7) and (8) are somewhat ambiguous on some scales. This leads to unphysical results on small scales that the cross-correlation factor $r_{\rm obj}$ does not lie in the range $[-1,1]$ and that the biasing factor $b_{\rm obj}$ may become imaginary. Indeed, this behavior $r_{\rm obj} \gtrsim 1$ shows up in the halo model (Figure 5). In the light of this, it is useful and instructive to relate our biasing parameters to those defined in terms of one-point statistics which are wel-defined on all scales.

In general, the two-point statistics does not simply reduce to the one-point statistics because of the difference of their smoothing function. Nevertheless in the case of the top-hat window function, the variances of mass, objects and their cross-correlation can be explicitly written in terms of the corresponding two-point correlation functions as follows:

$$\sigma_{ij}^2(R_{\rm TH}) = 4\pi \int_0^{2R_{\rm TH}} dr\ r^2\, \xi_{ij}(r)\ F(r;R_{\rm TH}), \tag{30}$$

where the subscripts i and j mean either o or m. The filter function $F(r;R_{\rm TH})$ is given by

$$F(r;R_{\rm TH}) = \frac{3}{\pi}\frac{(r-2R_{\rm TH})^2(r+4R_{\rm TH})}{(2R_{\rm TH})^6}, \tag{31}$$

and satisfies the normalization condition :

$$4\pi \int_0^{2R_{\rm TH}} dr\ r^2\, F(r;R_{\rm TH}) = 1. \tag{32}$$

Using the above relation, one can in principle reproduce the biasing and cross-correlation factors for one-point statistics in a straightforward manner. In practice, however, one has to take account of the finite resolution of the numerical data carefully. In particle simulations, the smallest scales are supposed to be dominated by the discreteness effect and the two-point correlation functions at $r=0$ are formally described by the sum of the Dirac delta function. In fact, this sensitively changes the amplitude of $\sigma_{ij}(R_{\rm TH})$ on small scales. This implies that one has to introduce a particular model of two-point correlation functions at $r=0$. For this purpose, we adopt the following procedure. We assume that the number density of each object on smallest scales is simply described by the sum of (randomly distributed) Dirac's delta function $n_{\rm obj}(x) = \sum_n \delta_D(x-x_n)$. In this case, the Poisson process yields the following offset to the intrinsic clustering term $\sigma_{ii}^2(R_{\rm TH})$:

$$\sigma_{ii,\rm true}^2(R_{\rm TH}) = \sigma_{ii}^2(R_{\rm TH}) + \sigma_{\rm shot}^2(R_{\rm TH}), \tag{33}$$

where the first term in the right-hand-side is calculated from equation (30) using the numerical data of correlation functions above the scales of the resolution. The second term is given by

$$\sigma_{\rm shot}^2(R_{\rm TH}) = \left[\frac{4\pi}{3} R_{\rm TH}^3 \overline{n}_{\rm obj}\right]^{-1}. \tag{34}$$

in the case of the top-hat window function with $\overline{n}_{\rm obj}$ being the mean number density of objects.

Adopting equation (33), we estimate the variances $\sigma_{ii,\rm true}$ and then compute the biasing parameters $b_{\rm obj}^{(1)}$ and $r_{\rm obj}^{(1)}$:

$$b_{\rm obj}^{(1)} \equiv \frac{\sigma_{\rm oo}}{\sigma_{\rm mm}}, \tag{35}$$

$$r_{\rm obj}^{(1)} \equiv \frac{\sigma_{\rm om}^2}{\sigma_{\rm oo}\sigma_{\rm mm}}, \tag{36}$$

where $\sigma_{\rm om} = \sqrt{\langle \delta_{\rm obj}\delta_{\rm mass}\rangle}$ is the one-point cross-correlation.

In Figures 7 and 8, the biasing parameters for the one-point statistics are shown as a function of smoothing radius $R_{\rm TH}$. On large scales, their behavior is similar to that for the two-point statistics, and the theoretical prediction is good agreement with the numerical results. On the other hand, on small scales, the point process dominates the clustering signal and scale-dependence of the biasing and cross-correlation factor is quite different from that of $b_{\rm obj}$ and $r_{\rm obj}$ for both peaks and halos; $r_{\rm obj}^{(1)}$ substantially deviates from unity and $b_{\rm obj}^{(1)}$ becomes quite large as the smoothing radius $R_{\rm TH}$ decreases. The effect becomes more significant in the redshift-space and/or at higher redshift, since the redshift-space distortion and redshift evolution tend to weaken the intrinsic clustering amplitude.

The comparison of those biasing parameters between the one- and two-point statistics suggests that our results are reliable on scales larger than $\sim 1h^{-1}$Mpc for peaks and $\sim 5h^{-1}$Mpc for halos where the small-scale modeling does not seriously affect the biasing parameters.

4. Conclusions and discussion

We have extensively examined the scale-dependence, time-evolution, and redshift-space distortion of biasing in peak and halo models, with particular attention to the nonlinear stochastic nature. Especially, we quantify the biasing properties defined in terms of the two-point statistics and the results are compared with those in the one-point statistics. Our main results are summarized as follows:

(1) We have quantitatively demonstrated the degree of nonlinearity and stochasticity of biasing in peak and halo models. In particular, biasing is significantly nonlinear and stochastic in nonlinear regimes of gravitational clustering, due to the gravitational evolution for peaks and volume exclusion for halos, which results in strong scale-dependence of the biasing parameters on small scales ($\lesssim$ a few Mpc).

(2) On scales larger than $10h^{-1}$Mpc, however, a linear deterministic and scale-independent biasing remains a reasonable approximation in peak and halo models. While the biasing parameters in this linear regime evolve as a redshift, their evolution is consistent with the existing theoretical model predictions.

(3) Redshift-space distortion of the biasing on small scales is quite different in peak and halo models because the pair-wise velocity dispersions are quite sensitive to those objects. This difference affects the stochasticity of biasing in redshift space. The linear redshift-space distortion, on the other hand, is very similar and explained by extending the model of Kaiser (1987) to the stochastic biasing case (see Appendix).

The biasing models considered here are rather idealistic for the observed luminous objects which form through the complicated processes including the gas dynamics and the radiative transfer. Nevertheless the peak and halo models contain the most important aspect of the formation of astrophysical objects, the nonlinear gravitational growth and the subsequent merging, in the scenario of hierarchical galaxy formation. This is why our results are qualitatively similar to the recent numerical work of Cólin et al. (1999) and Somerville et al. (1999), and also to predictions of an analytical model of Taruya & Suto (2000). Moreover cosmological simulations of galaxy formation by Yoshikawa et al. (2000) indicate that the one-to-one correspondence between halos and galaxies may be a reasonably good approximation on large scales and the nonlinear clustering of peaks traces the galaxy distribution fairly well even on small scales.

The validity of linear deterministic and scale-independent relation on large scales may be a natural consequence of the hierarchical clustering scenario (e.g., Matsubara 1999). Such scale-independence probably comes from the fact that the statistical feature of large-scale clustering of peaks and halos is simply characterized by a single parameter; the mass threshold M for halos and the density height ν for peaks. Our important result is that the relation $\delta_{\rm obj} \simeq b_{\rm obj}\delta_{\rm mass}$ still holds in quasi-linear regime. If this is the case, the interpretation of clustering of realistic objects is straightforward. On the other hand, the scale-dependence of the biasing becomes crucial in the nonlinear regime of density fluctuations. These should be kept in mind in interpreting the future redshift surveys of galaxies.

We thank Ue-Li Pen, for pointing out the importance of the relation between the one- and two-point statistics (eq.[30]), which improves our analysis and leads to the discussion in Section 3.4. Y. P. J. and A.T. gratefully acknowledge support from a JSPS (Japan Society for the Promotion of Science) fellowship. Numerical computations were carried out on VPP300/16R and VX/4R at ADAC (the Astronomical Data Analysis Center) of the National Astronomical Observatory, Japan, as well as at RESCEU (Research Center for the Early Universe, University of Tokyo) and KEK (High Energy Accelerator Research Organization, Japan). This research was supported in part by the Grant-in-Aid by the Ministry of Education, Science, Sports and Culture of Japan (07CE2002, 12640231) to RESCEU, and by the Supercomputer Project (No.99-52, No.00-63) of KEK.

Appendix. Linear stochastic biasing in redshift-space

This appendix describes the generalization of the the linear redshift-space distortion model of Kaiser (1987) in the context of the stochastic biasing. Although we consider the biasing for the one-point statistics, the results are also applicable to the biasing for two-point statistics as long as the correlation functions are positive.

First recall that the density contrast of dark matter and objects in k-space is given by

$$\delta^{(\rm S)}_{\rm mass}(\mathbf{k}) = \delta^{(\rm R)}_{\rm mass}(\mathbf{k}) + f\mu^2\delta^{(\rm R)}_{\rm mass}(\mathbf{k}), \tag{A1}$$

$$\delta^{(\rm S)}_{\rm obj}(\mathbf{k}) = \delta^{(\rm R)}_{\rm obj}(\mathbf{k}) + f\mu^2\delta^{(\rm R)}_{\rm mass}(\mathbf{k}), \tag{A2}$$

where $\mu = k_\parallel/k$ is the direction cosine in k-space ($k_\parallel$ is the comoving wave number parallel to the line of sight), and

$$f \equiv \frac{d\ln D(z)}{d\ln a} \simeq \Omega(z)^{0.6} + \frac{\lambda(z)}{70}\left(1+\frac{\Omega(z)}{2}\right), \tag{A3}$$

$$\Omega(z) = \left[\frac{H_0}{H(z)}\right]^2 (1+z)^3\,\Omega_0, \tag{A4}$$

$$\lambda(z) = \left[\frac{H_0}{H(z)}\right]^2 \lambda_0\,. \tag{A5}$$

Equations (A1) and (A2), relate the auto- and cross-correlation functions in redshift space to those in real space:

$$\langle\delta^{(\mathrm{S})}_{\mathrm{mass}}\delta^{(\mathrm{S})}_{\mathrm{mass}}\rangle(\mu) = \left(1+2f\mu^2+f^2\mu^4\right)\langle\delta^{(\mathrm{R})}_{\mathrm{mass}}\delta^{(\mathrm{R})}_{\mathrm{mass}}\rangle, \tag{A6}$$

$$\langle\delta^{(\mathrm{S})}_{\mathrm{obj}}\delta^{(\mathrm{S})}_{\mathrm{obj}}\rangle(\mu) = \left(1+2\beta r^{(\mathrm{R})}_{\mathrm{obj}}\mu^2+\beta^2\mu^4\right)\langle\delta^{(\mathrm{R})}_{\mathrm{obj}}\delta^{(\mathrm{R})}_{\mathrm{obj}}\rangle, \tag{A7}$$

$$\langle\delta^{(\mathrm{S})}_{\mathrm{mass}}\delta^{(\mathrm{S})}_{\mathrm{obj}}\rangle(\mu) = \left[b^{(\mathrm{R})}_{\mathrm{obj}}r^{(\mathrm{R})}_{\mathrm{obj}}+f\mu^2\left(1+b^{(\mathrm{R})}_{\mathrm{obj}}r^{(\mathrm{R})}_{\mathrm{obj}}\right)+f^2\mu^4\right]\langle\delta^{(\mathrm{R})}_{\mathrm{mass}}\delta^{(\mathrm{R})}_{\mathrm{mass}}\rangle, \tag{A8}$$

where the brackets indicate the ensemble average, $\beta \equiv f/b^{(\mathrm{R})}_{\mathrm{obj}}$ and the quantities $b^{(\mathrm{R})}_{\mathrm{obj}}$ and $r^{(\mathrm{R})}_{\mathrm{obj}}$ denote the biasing and cross-correlation factors in real space:

$$b^{(\mathrm{R})}_{\mathrm{obj}} \equiv \sqrt{\frac{\langle\delta^{(\mathrm{R})}_{\mathrm{obj}}\delta^{(\mathrm{R})}_{\mathrm{obj}}\rangle}{\langle\delta^{(\mathrm{R})}_{\mathrm{mass}}\delta^{(\mathrm{R})}_{\mathrm{mass}}\rangle}}, \tag{A9}$$

$$r^{(\mathrm{R})}_{\mathrm{obj}} \equiv \frac{\langle\delta^{(\mathrm{R})}_{\mathrm{mass}}\delta^{(\mathrm{R})}_{\mathrm{obj}}\rangle}{\sqrt{\langle\delta^{(\mathrm{R})}_{\mathrm{mass}}\delta^{(\mathrm{R})}_{\mathrm{mass}}\rangle\langle\delta^{(\mathrm{R})}_{\mathrm{obj}}\delta^{(\mathrm{R})}_{\mathrm{obj}}\rangle}}. \tag{A10}$$

The biasing and cross-correlation factors in redshift space are defined similarly using equations (A6)-(A8). After integrating over μ, we find

$$b^{(\mathrm{S})} \equiv \sqrt{\frac{\langle\delta^{(\mathrm{S})}_{\mathrm{obj}}\delta^{(\mathrm{S})}_{\mathrm{obj}}\rangle}{\langle\delta^{(\mathrm{S})}_{\mathrm{mass}}\delta^{(\mathrm{S})}_{\mathrm{mass}}\rangle}} = b^{(\mathrm{R})}_{\mathrm{obj}}\sqrt{\frac{(1+\frac{2}{3}\beta r^{(\mathrm{R})}_{\mathrm{obj}}+\frac{1}{5}\beta^2)}{(1+\frac{2}{3}f+\frac{1}{5}f^2)}}, \tag{A11}$$

$$r^{(\mathrm{S})}_{\mathrm{obj}} \equiv \frac{\langle\delta^{(\mathrm{S})}_{\mathrm{mass}}\delta^{(\mathrm{S})}_{\mathrm{obj}}\rangle}{\sqrt{\langle\delta^{(\mathrm{S})}_{\mathrm{mass}}\delta^{(\mathrm{S})}_{\mathrm{mass}}\rangle\langle\delta^{(\mathrm{S})}_{\mathrm{obj}}\delta^{(\mathrm{S})}_{\mathrm{obj}}\rangle}} = \frac{r^{(\mathrm{R})}_{\mathrm{obj}}+\frac{1}{3}\beta(1+b^{(\mathrm{R})}_{\mathrm{obj}}r^{(\mathrm{R})}_{\mathrm{obj}})+\frac{1}{5}f\beta}{\sqrt{(1+\frac{2}{3}f+\frac{1}{5}f^2)(1+\frac{2}{3}\beta r^{(\mathrm{R})}_{\mathrm{obj}}+\frac{1}{5}\beta^2)}}. \tag{A12}$$

In the deterministic case $r^{(R)}_{\mathrm{obj}} = 1$, one can show that

$$b^{(S)}_{\mathrm{obj}} \le b^{(R)}_{\mathrm{obj}}, \tag{A13}$$

$$r^{(S)}_{\mathrm{obj}} \le r^{(R)}_{\mathrm{obj}} = 1, \tag{A14}$$

from equations (A11) and (A12). The inequality (A13) is understood by the squashing effect which is more appreciable for $\delta^{(S)}_{\mathrm{mass}}$ if $\delta^{(R)}_{\mathrm{obj}} > \delta^{(R)}_{\mathrm{mass}}$ (see eqs.[A1] and [A2]). The inequality (A14) merely reflects the fact that the random peculiar velocity generates an additional scatter around the mean biasing relation in redshift space.

In a more general case, the biasing is not deterministic i.e., $r^{(R)}_{\mathrm{obj}} < 1$. Even then the inequality (A13) still holds as long as $b^{(R)}_{\mathrm{obj}} > 1$ and $r^{(R)}_{\mathrm{obj}} \le 1$. The inequality (A14), on the other hand, no longer holds, and in fact, the opposite inequality seems to be a fairly general result; Figure 9 plots $r^{(S)}_{\mathrm{obj}} - r^{(R)}_{\mathrm{obj}}$ as a function of $r^{(R)}_{\mathrm{obj}}$ for different values of f; $f = 0.3$ (solid lines), $f = 0.6$ (dashed lines), and 0.9 (dotted lines) with $b^{(R)}_{\mathrm{obj}} = 3.0$ (*left-panel*) and $b^{(R)}_{\mathrm{obj}} = 5.0$ (*right-panel*). Except for a small region around $r^{(R)}_{\mathrm{obj}} \simeq 1$, $r^{(S)}_{\mathrm{obj}}$ is generally *larger* than $r^{(R)}_{\mathrm{obj}}$. It seems that the stochasticity is effectively reduced due to the redshift-space distortion as increasing the stochasticity in real space. Moreover this tendency becomes stronger when the factor f becomes large, or equivalently, the density parameter Ω_0 approaches unity.

Thus in linear theory of redshift-space distortion, we conclude fairly generally that $b^{(S)}_{\mathrm{obj}} \le b^{(R)}_{\mathrm{obj}}$ and $r^{(S)}_{\mathrm{obj}} \gtrsim r^{(R)}_{\mathrm{obj}}$ as long as a certain degree of the stochascity exists in real space (i.e., $r^{(R)}_{\mathrm{obj}} < 1$) as Figure 9 exhibits.

References

Bardeen J.M., Bond J.R., Kaiser N., Szalay, A.S. 1986, ApJ 304, 15
Blanton M., Cen R.Y., Ostriker J.P., Strauss M.A. 1999, ApJ 522, 590
Blanton M., Cen R.Y., Ostriker J.P., Strauss M.A., Tegmark M. 2000, ApJ 531, 1
Cólin P., Klypin A.A., Kravtsov A.V., Khokhlov A. 1999, ApJ 523, 32
Dekel A., Lahav O. 1999, ApJ 520, 24
Fry J.N. 1996, ApJL 461, 65
Hamilton A.J.S. 1998, in Proceedings of Ringberg Workshop on Large-Scale Structure, Hamilton, D.(ed.), Kluwer Academic, Dordrecht, p.185
Jing Y.P. 1998, ApJL 503, 9
Jing Y.P., Suto Y. 1998,ApJL 494, 5
Kaiser N. 1984, ApJL 284, 9
Kaiser N. 1987, MNRAS 227, 1
Kitayama T., Suto Y. 1997, ApJ 490, 557
Matsubara T. 1999, ApJ 525, 543
Mo H.J., White, S.D M. 1996, MNRAS 282, 347
Mo H.J., Jing Y.P., White, S.D.M. 1997, MNRAS 284, 189
Peebles P.J.E. 1980, The Large Scale Structure of the Universe, Princeton University Press
Pen U.L. 1998, ApJ 504, 601
Press W.H., Schechter P. 1974, ApJ 187, 425
Somerville R.S., Lemson G., Sigad Y., Dekel A., Kauffmann G., White S.D.M. 1999, preprint (astro-ph/9912073)
Taruya A. 2000, ApJ 537, 37
Taruya A., Koyama K, Soda J. 1999,ApJ 510, 541
Taruya A., Soda J. 1999, ApJ 522, 46
Taruya A., Suto Y. 2000, ApJ 542, 559
Tegmark M., Peebles P.J.E. 1998, ApJL 500, 79
Tegmark M., Bromley B. 1999, ApJL 518, 69
Yoshikawa K., Taruya A., Jing Y.P., Suto Y. 2000, ApJ, submitted

Table 1. Simulation model parameters.

Model	Ω_0	λ_0	$\Gamma^\dagger$	σ_8	N	$m_{\rm p}^\ddagger[h^{-1}{\rm M}_\odot]$	realizations
SCDM (Standard CDM)	1.0	0.0	0.5	0.6	256^3	4.5×10^{11}	3
LCDM (Lambda CDM)	0.3	0.7	0.21	1.0	256^3	1.3×10^{11}	3
OCDM (Open CDM)	0.3	0.0	0.25	1.0	256^3	1.3×10^{11}	3

† the shape parameter of the power spectrum.
‡ mass of a single dark matter particle.

Table 2. The peak catalogue.

	SCDM		LCDM		OCDM	
$\nu_{\rm th}$	$N^\dagger$	$b^\ddagger_{\rm peak,eff}$	N	$b_{\rm peak,eff}$	N	$b_{\rm peak,eff}$
1.0	6.2×10^5	1.2 (1.8)	5.3×10^5	1.2 (1.5)	5.5×10^5	1.2 (1.4)
2.0	2.6×10^5	1.6 (2.8)	2.2×10^5	1.5 (2.2)	2.3×10^5	1.5 (1.9)
3.0	5.0×10^4	2.0 (4.1)	4.5×10^4	1.8 (3.1)	4.6×10^4	1.8 (2.6)

† average total number of peaks among three realizations.
‡ effective biasing factor of peaks at $z=0.0$ ($z=2.2$).

Table 3. The halo catalogue.

	SCDM		LCDM		OCDM	
$M_{\rm th}[h^{-1}{\rm M}_\odot]$	$N^\dagger$	$b^\ddagger_{\rm halo,eff}$	N	$b_{\rm halo,eff}$	N	$b_{\rm halo,eff}$
2×10^{12}	——— (———)	1.1 (5.2)	7.3×10^4 (3.9×10^4)	0.9 (2.6)	8.2×10^4 (6.6×10^4)	0.9 (1.8)
5×10^{12}	1.2×10^5 (1.4×10^4)	1.1 (5.2)	3.0×10^4 (1.1×10^4)	1.0 (3.3)	3.4×10^4 (2.1×10^4)	1.0 (2.3)
1×10^{13}	5.7×10^4 (2.3×10^3)	1.3 (6.7)	1.5×10^4 (3.3×10^3)	1.2 (4.1)	1.7×10^4 (8.3×10^4)	1.2 (2.8)

† average total number of halos among three realizations at $z=0.0$ ($z=2.2$).
‡ effective biasing factor of halos at $z=0.0$ ($z=2.2$).

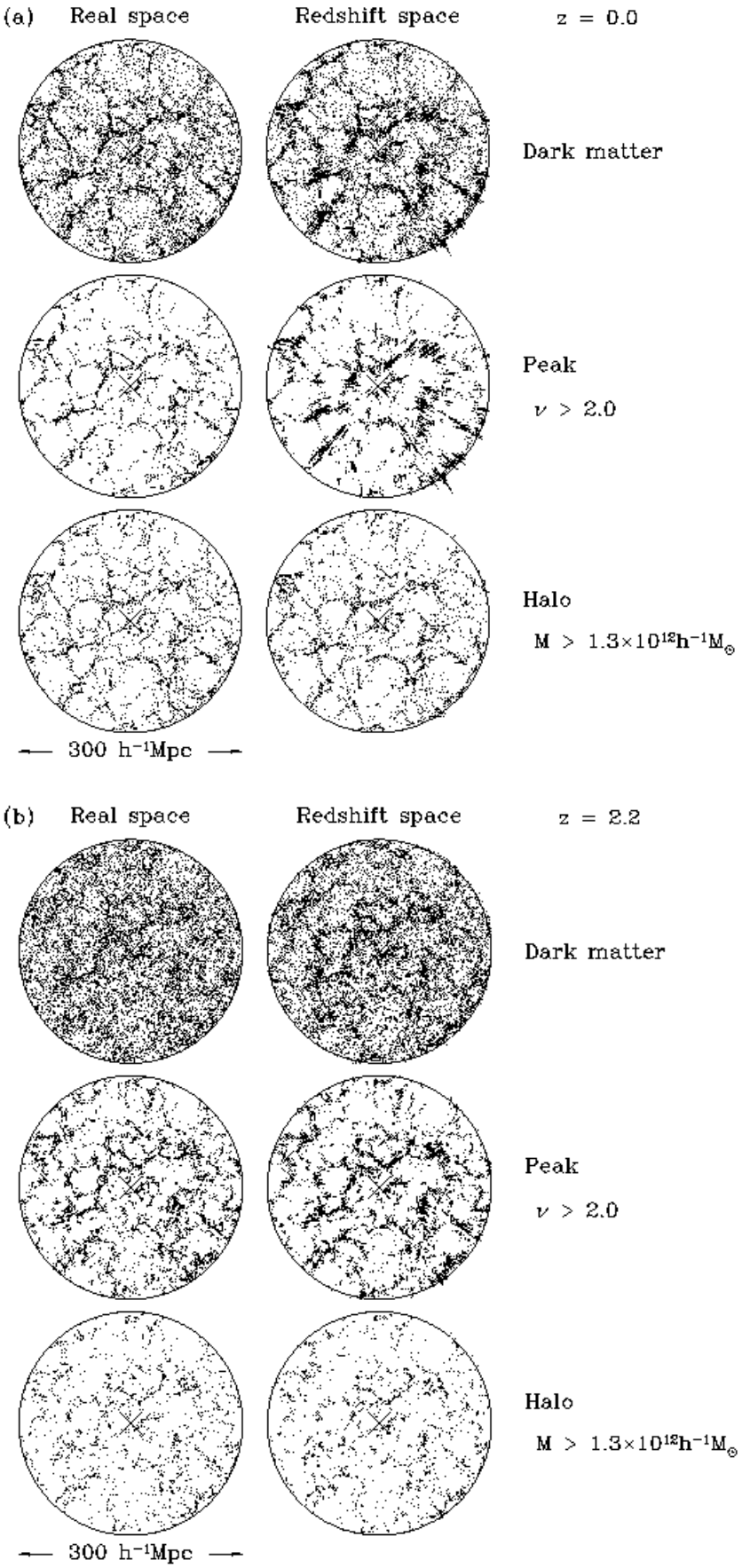

Fig. 1.. Top-view of distribution of objects in real (left panels) and redshift (right panels) spaces around the fiducial observer at the center; dark matter particles (top panels), peaks with $\nu > 2$ (middle panels) and halos with $M > 1.3 \times 10^{12} \mathrm{M}_{\odot}$ (bottom panels) in LCDM model. The thickness of those slices is $15h^{-1}$Mpc; (a) $z = 0$, (b) $z = 2.2$.

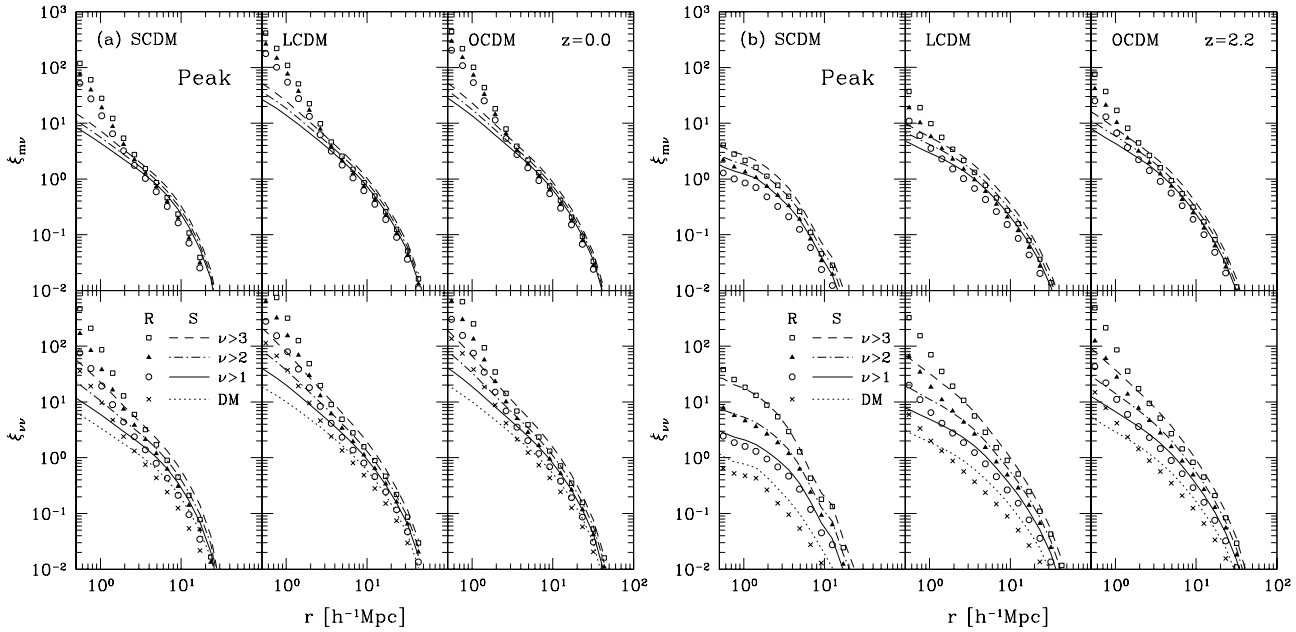

Fig. 2.. Auto- and cross-correlation functions of dark matter and peaks in SCDM (left panels), LCDM (middle panels) and OCDM (right panels). Different symbols indicate the results in real space (open squares for $\nu > 3$, filled triangles for $\nu > 2$, open circles for $\nu > 1$, and crosses for dark matter), while different curves indicate those in redshift space (dashed for $\nu > 3$, dot–dashed for $\nu > 2$, solid for $\nu > 1$, and dotted for dark matter). (a) $z = 0$, (b) $z = 2.2$.

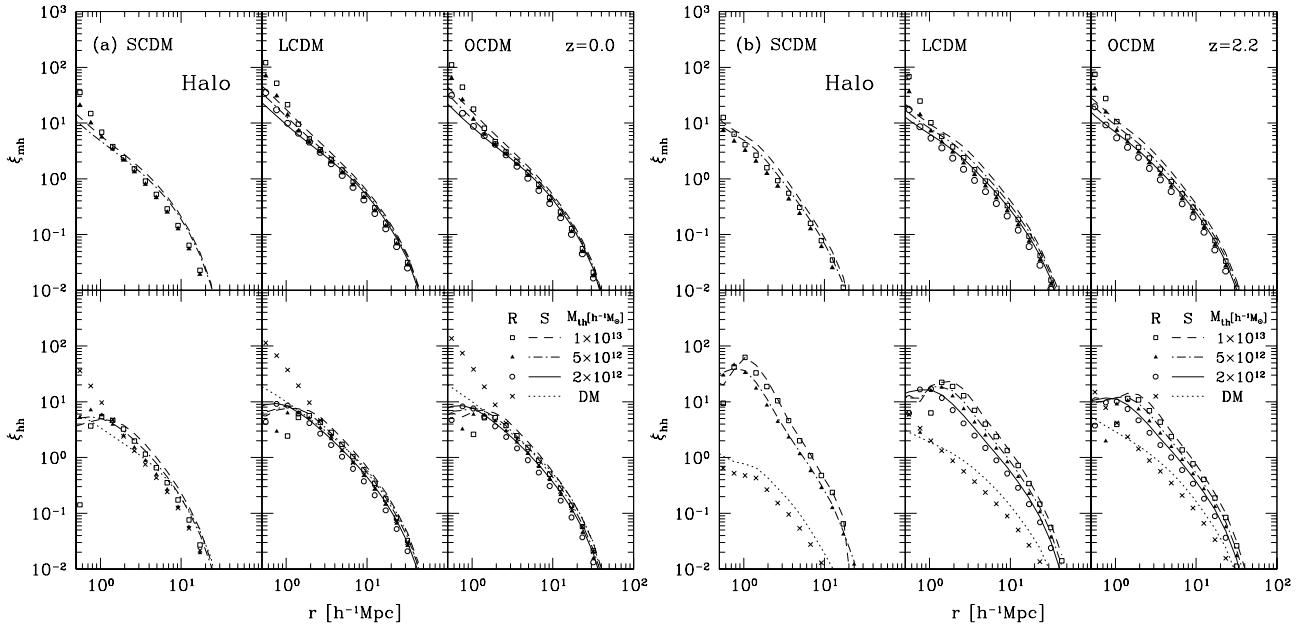

Fig. 3.. Same as Fig. 2 but for halo model; open squares and dashed lines for $M > 10^{13}h^{-1}M_{\odot}$, filled triangles and dot–dashed lines for $M > 5 \times 10^{12}h^{-1}M_{\odot}$, open circles and solid lines for $M > 2 \times 10^{12}h^{-1}M_{\odot}$, and crosses and dotted lines for dark matter. For SCDM model, we only plot the correlation functions with $M_{\rm th} = 5 \times 10^{12},\ 10^{13}h^{-1}M_{\odot}$. (a) $z = 0$, (b) $z = 2.2$.

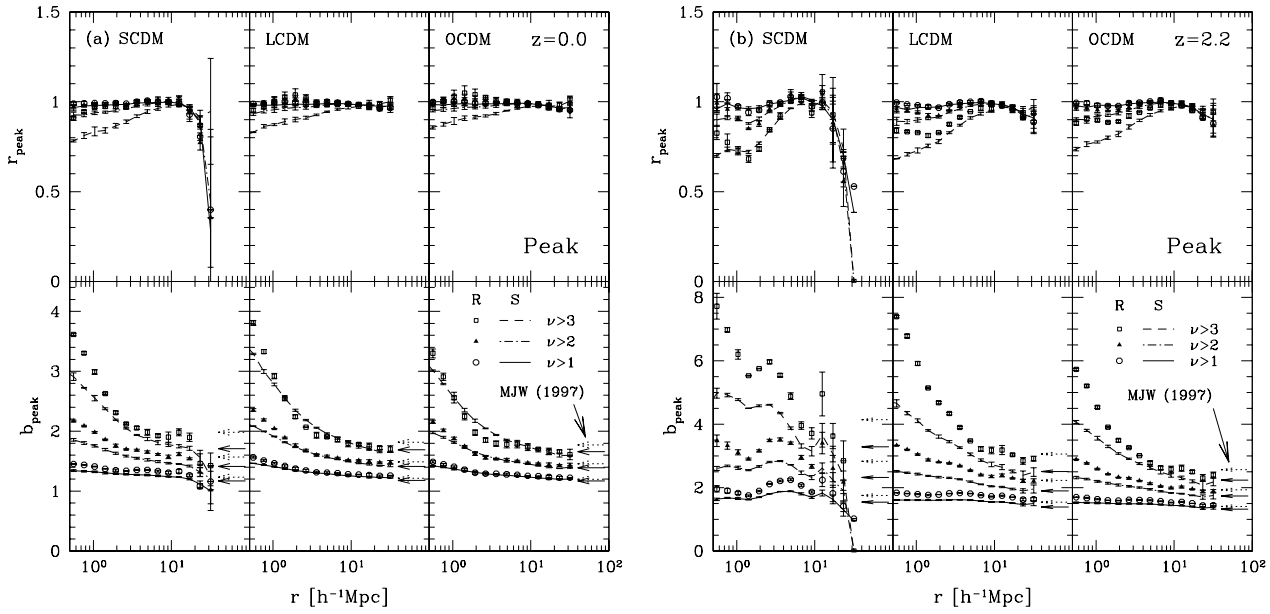

Fig. 4.. Scale-dependence of the biasing and cross-correlation factors for two-point statistics of peak model. Different symbols and lines have the same meaning as in Fig.2. The arrows in the bottom panels indicate the model predictions of Mo, Jing, & White (1997) in real (dotted) and redshift (solid) spaces. (a) $z = 0$, (b) $z = 2.2$.

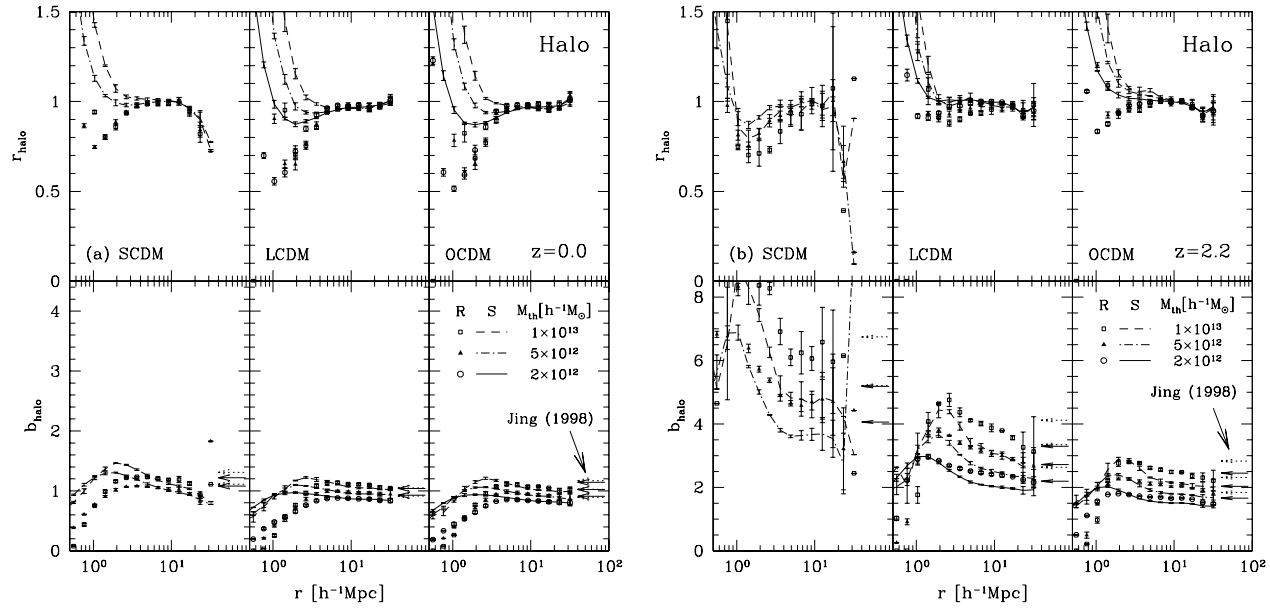

Fig. 5.. Same as Fig. 4, but for halo model. Different symbols and lines have the same meaning as in Fig.3. The arrows in the bottom panels indicate the model predictions of Jing (1998) in real (dotted) and redshift (solid) spaces. (a) $z = 0$, (b) $z = 2.2$.

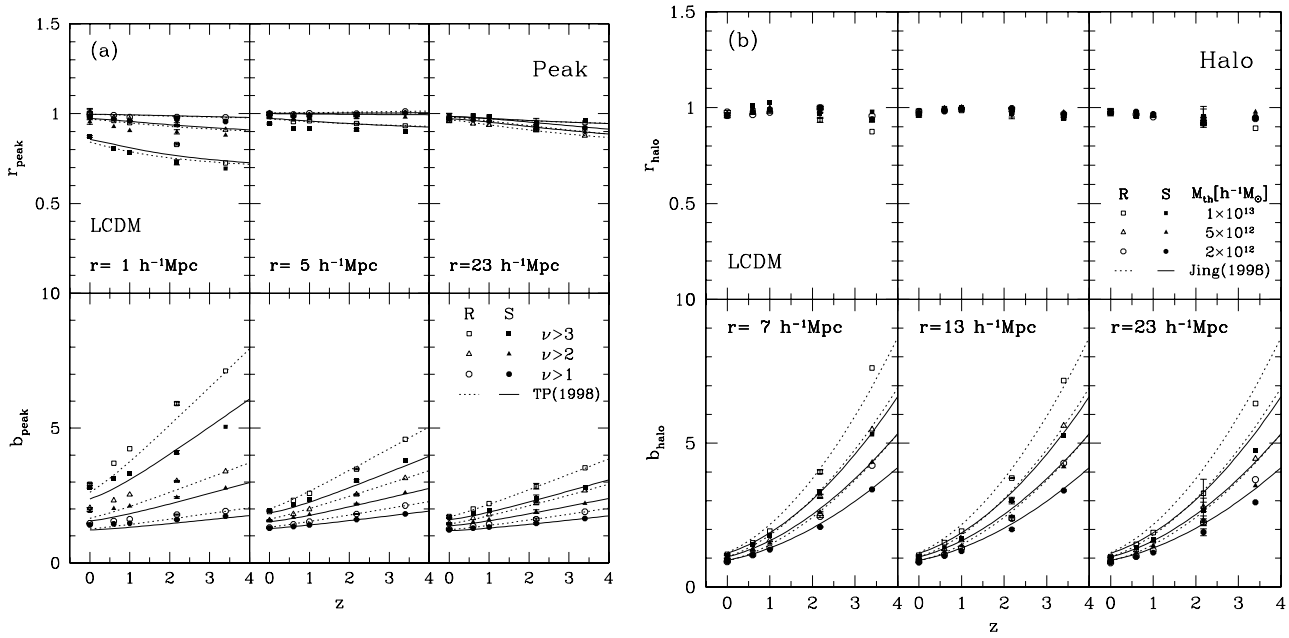

Fig. 6.. Time evolution of the biasing and cross-correlation factors in LCDM model. (a) Open (filled) symbols indicate the peak simulation results for $\nu > 3$ (squares), $\nu > 2$ (triangles), and $\nu > 1$ (circles) peaks in real (redshift) spaces. Dotted and solid lines correspond to the model predictions of Tegmark & Peebles (1998) in real and redshift spaces, respectively, normalized by the data at $z = 3.4$. (b) Open (filled) symbols indicate the halo simulation results for $M > 10^{13}h^{-1}M_\odot$ (squares), $M > 5 \times 10^{12}h^{-1}M_\odot$ (triangles), and $M > 2 \times 10^{12}h^{-1}M_\odot$ (circles) peaks in real (redshift) spaces. Dotted and solid curves correspond to the model prediction of Jing (1998) in real and redshift spaces, respectively. (b) halo model.

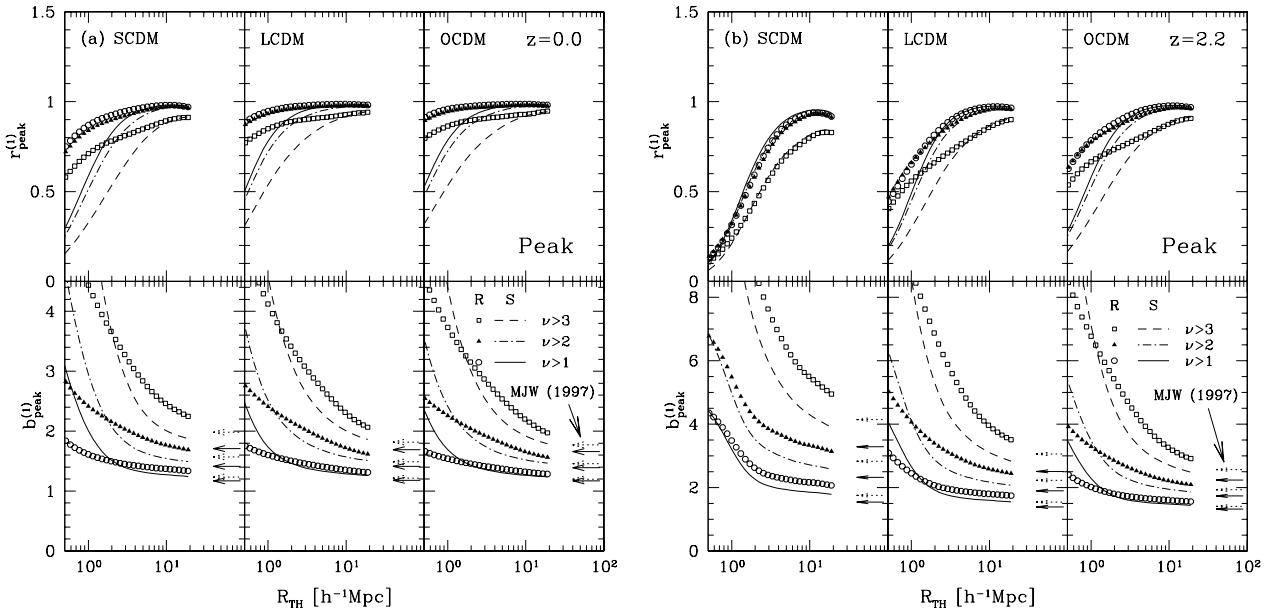

Fig. 7.. Scale-dependence of the biasing and cross-correlation factors for one-point statistics of peak model. Different symbols and lines have the same meaning as in Fig.2. The arrows in the bottom panels indicate the same model predictions as in Fig.4. (a) $z = 0$, (b) $z = 2.2$.

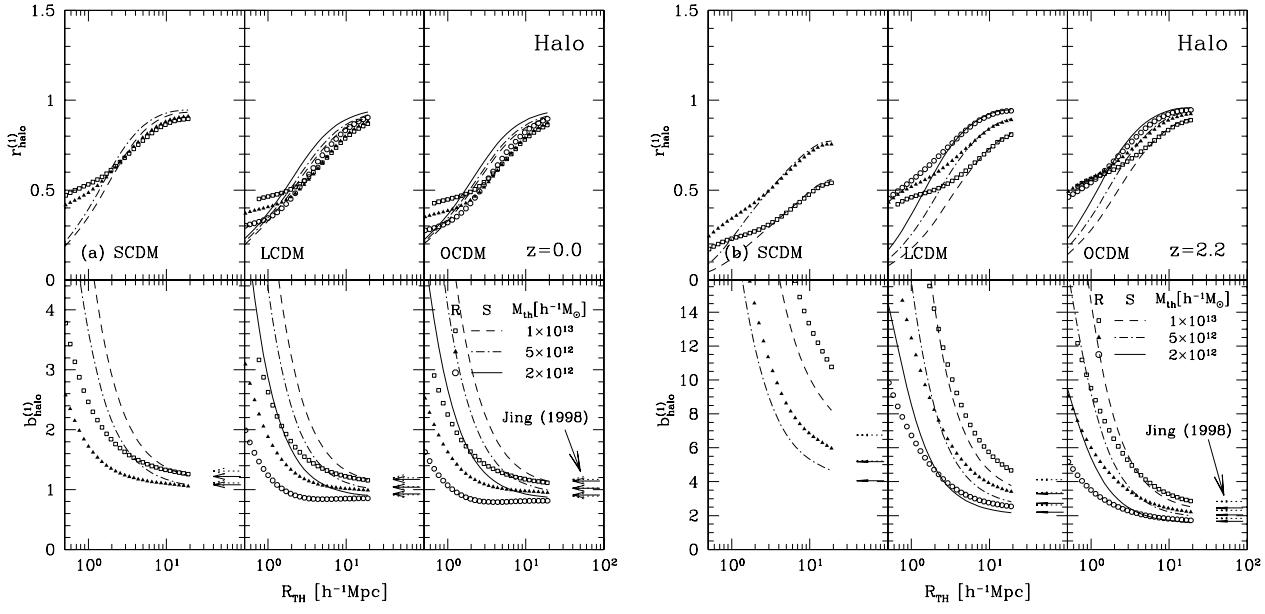

Fig. 8.. Same as FIg. 7, but for halo model. Different symbols and lines have the same meaning as in Fig.3. The arrows in the bottom panels indicate the same model predictions as in Fig.5. (a) $z = 0$, (b) $z = 2.2$.

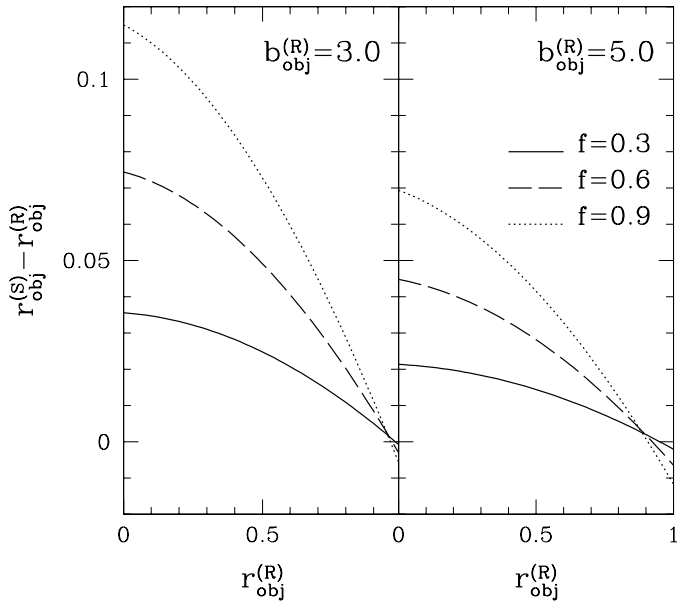

Fig. 9.. The difference $r_{\rm obj}^{(S)} - r_{\rm obj}^{(R)}$ as a function of $r_{\rm obj}^{(R)}$ for $f = 0.3$ (solid), $f = 0.6$ (dashed), and 0.9 (dotted) with $b_{\rm obj}^{(R)} = 3.0$ (*left-panel*) and $b_{\rm obj}^{(R)} = 5.0$ (*right-panel*).